Simple homogenized model for the non-linear analysis of FRP strengthened masonry structures. Part II: structural applications

Gabriele Milani[(1)], Paulo B. Lourenço[(2)]

(1) Corresponding Author. Dipartimento di Ingegneria Strutturale (DIS), Politecnico di Milano, Piazza Leonardo da Vinci 32, 20133 Milano, Italy. E-mail: milani@stru.polimi.it
(2) ISISE, Department of Civil Engineering, School of Engineering, University of Minho, Azurém, 4800-058 Guimaraes, Portugal

Keywords: Masonry, FRP strengthening, non-linear behavior, in- and out-of-plane loads, 3D structural analysis, curved shells

Abstract

The homogenized masonry non-linear stress-strain curves obtained through the simple micro-mechanical model developed in the first part of the paper are here used for the analysis of strengthened masonry walls under various loading conditions. In particular, a deep beam and a shear wall strengthened with FRP strips are analyzed for masonry loaded in-plane. Additionally, single and double curvature masonry structures strengthened in various ways, namely a circular arch with buttresses and a ribbed cross vault are considered. For all the examples presented, both the non-strengthened and FRP strengthened cases are discussed. Additional non-linear FE analyses are performed, modeling masonry through an equivalent macroscopic material with softening, in order to assess the present model predictions. Detailed comparisons between the experimental data, where available, and numerical results are also presented. The examples show the efficiency of the homogenized technique with respect to: (1) accuracy of the results; (2) low number of finite elements required; (3) independence of the mesh, at a structural level, from the actual texture of masonry.

1. Introduction

The low resistance of masonry under horizontal loads is a well-known matter for all technicians and practitioners involved in the safety assessment of historical city centers (Ramos and Lourenço 2004, Yi et al. 2006, Moon et al. 2007). The need for designing efficient and non-invasive strengthening interventions appears therefore one of the key issues to be resolved by engineers involved in the repair and/or rehabilitation of masonry buildings before and after earthquakes. FRP strengthening seems as an interesting solution for masonry upgrading because the technique is able to substantially improve the load bearing capacity of brickwork structures.

The most important effect of a generic strengthening intervention executed with externally bonded FRP strips is to preclude the formation of the failure mechanism which causes the collapse of the non-strengthened structure, Foraboschi (2004). The objective is the formation of a new collapse mechanism different from the un-strengthened case, with higher internal dissipation. Obviously, ‘‘hand” calculations are not enough in general and may not be performed easily for complex structures, especially in the presence of curved shells with unsymmetrical loads.

At the same time, despite the great importance and the increasing diffusion of FRP strengthening, a robust, easy to use and general non-linear numerical model able to give predictions beyond the linear elastic range on the behavior of FRP-strengthened masonry with any shape and under various loading conditions seems still lacking. Ideally, to be fully predictive, a numerical model should take into account a number of important structural aspects, exhibited by strengthened masonry at low levels of the external loads and at the verge of collapse, which are:

1. The low masonry resistance against tensile stresses, due to the insufficient capacity of mortar joints to behave elastically in the tension range.
2. The orthotropy in both the elastic and inelastic range, Lourenço (2000), Massart et al. (2004). Orthotropy is significantly related to the texture of the masonry, both for in- and out-of-plane actions. For horizontal stretching and horizontal bending, i.e. out-of-plane flexion

with rotation along a vertical axis (Mercatoris et al. 2009, Milani & Lourenço 2010), the masonry texture produces perceivable effects that tend to become more evident with the progressive degradation of the material. The different topology of the continuous horizontal mortar joints with respect to the vertical joints, interrupted by the blocks, implies that the shear response of the mortar plays a key role.

3. The delamination of the FRP from the support (e.g. Triantafillou 1998, Luciano & Sacco 1998, Marfia & Sacco 2001). Delamination is typically brittle, and depends on many concurring factors, such as material and adhesive bulk properties, surface conditions, possible chemical–physical treatments before the FRP application, and environmental conditions (temperature and humidity during and after the strengthening intervention).

Conversely, to be efficient, a structural model should avoid a micro-modeling representation, which would require prohibitive computational costs. As discussed in the accompanying paper (Part I), a suitable way for the analysis of FRP strengthened walls is a two-step approach based on homogenization concepts. The first step, relying in the simplified homogenization of non-strengthened masonry, with a curved and flat representative volume element, has been widely illustrated in Part I, and the reader is referred there for a proper discussion of the limitations and the capabilities of the method.

In the present Part II, macroscopic non-linear stress-strain relationships obtained in Part I are implemented in a structural non-linear FE code for the realistic analysis of FRP strengthened masonry flat and curved structures beyond the linear elastic range. As already discussed in Part I, rigid infinitely resistant wedge-shaped 3D elements interconnected by non-linear interfaces are used to model masonry at structural level. The utilization of 3D elements is suitable to simulate the flexural strength (Korany & Drysdale 2007, Mosallam 2007) increase obtained by the introduction of FRP strips. On the other hand, wedge-shaped elements are utilized with the aim of reproducing possible diagonal out-of-plane failures, due to the development of cracks (caused by bending and torsion) which zigzag between contiguous bricks. FRP strips are modeled by means of triangular

rigid elements. Masonry and FRP layers interact by means of interfacial tangential actions between triangles (FRP) and wedges (masonry). Furthermore, a possible limited tensile strength for the FRP strengthening is considered at the interfaces between adjoining triangular elements. Since delamination is a typical fragile phenomenon, an elastic behavior followed by a degradation of the strength until zero in correspondence of a pre-defined slip is assumed in the structural scale problem, following formulas provided by the recent Italian norm CNR-DT 200 (2004), see also Fedele & Milani (2011) and the simplifications discussed in Part I (linear piecewise constant approximation). In this way, delamination phenomenon at the FRP/masonry interface and FRP tensile failure may be taken into account.

In the paper, a deep beam and a shear wall strengthened with FRP strips are analyzed for masonry loaded in-plane. Additionally, single and double curvature masonry structures strengthened in various ways, namely a circular arch with buttresses and a ribbed cross vault are considered. For the examples presented, both the non-strengthened and FRP strengthened case are discussed. Detailed comparisons between the experimental data, where available, and numerical results are also presented. In order to further assess the reliability of the procedure proposed, results obtained through alternative non-linear FE analyses conducted by means of commercial codes (namely ANSYS 2004 and DIANA 2008) are also reported, where a non-linear elasto-plastic model exhibiting softening is assumed for masonry. Additionally, triangular interface elements with brittle behavior reproducing delamination of the strips from the support are adopted to model masonry-FRP bond. Non-linear FE analysis provides a valuable reference to compare with the present model results, in absence of experimental data available.

The examples show the efficiency of the proposed homogenized technique with respect to: (1) accuracy of the results; (2) reduced number of finite elements required; (3) independence of the mesh, at a structural level, from the actual texture of masonry.

2. Structural examples: in-plane loaded strengthened panels

The first and second structural examples analyzed consist of brickwork panels loaded in-plane, both in absence and presence of FRP strengthening disposed in various ways. The first example is a squat masonry deep beam tested at the University of Florence, Italy –experimental data are available in Grande et al. (2008)- and strengthened with diagonal and horizontal FRP strips, whereas the second example is a shear wall tested by Zhao et al. (2004). In this case a large diagonal strengthening is disposed on the lateral surfaces to increase considerably the shear load carrying capacity.

2.1. Deep beam

Three masonry panels with and without CFRP strips strengthening, denoted as PAN-A, are here examined, Figure 1. All panels, built with ¼ of common solid clay Italian bricks (dimensions 62.5 × 30 × 14 mm), have dimensions 290 × 270 mm (base × height). PAN-A is the non-strengthened wall, whereas PAN-A1 and PAN-A2 are specimens strengthened with different CFRP strip arrangements: a single horizontal strip for PAN-A1 and two symmetrical diagonal strips for PAN-A2. For these panels, several results are available, see Grande et al. (2008). The experimental tests were performed statically increasing the vertical external load applied at the top edge. The obtained results in terms of force-displacement diagrams (i.e. vertical load applied versus displacement of the steel plate that transfers the load to the panel) show key aspects induced by the CFRP strengthening on the global response of the panels. Furthermore, the examination of the crack paths during and after the tests shows important information on the effectiveness of the numerical model here proposed and on the contribution of the strengthening.

Mechanical properties of the masonry panels are reported in the companying paper and are not recalled here for the sake of conciseness. In order to experimentally determine such properties, uniaxial compression tests were conducted on bricks, mortar and masonry specimens according to the indications of the Italian code of practice D.M. 20/11/1987 (1987). The strengthening is

128 constituted by high-strength carbon fiber sheets. FRP parameters adopted in the model have been
129 deduced from experimental tests and from theoretical considerations, making use of CNR-DT200
130 (2004). Since no information on the fracture energy and the post peak parameters for mortar were
131 available, they are chosen according to the experimental results obtained by - Van der Pluijm (1992)
132 on masonry specimens characterized by similar mechanical properties. The joints compressive
133 strength f_c adopted in the numerical simulations is assumed equal to the experimental masonry
134 compressive strength value as all the non linearity is concentrated on interfaces, see Part I. For what
135 concerns the mechanical parameters adopted for FRP/masonry triangular interfaces, a fracture
136 energy equal to that evaluated using CNR DT-200 (2004) recommendations is adopted.
137 It is worth noting that, see Figure 1, all series were placed on steel plates of length L_s equal to 40
138 mm, disposed at the lower edge extremes and positioned on steel rollers allowing rotation of the
139 supports. The rotation of the lower edge extremes has minor effect on the numerical results, Grande
140 et al. (2008), and is not considered here for the sake of simplicity.
141 Experimental load-displacement curves for the three series of panels here analyzed, see Figure 2,
142 show that the introduction either of a horizontal strengthening (PAN-A1) or a double diagonal
143 strengthening (PAN-A2) results in a considerable increase of the ultimate load.
144 In Figure 2, (i) the force-displacement curves of the point of application of the external load (center
145 of the steel plate) from the two-step approach proposed, (ii) the ultimate load from an upper bound
146 FE limit analysis software derived directly from the present one assuming interfaces rigid-plastic
147 and (iii) the experimental force-displacement curves are reported for all the panels. Additionally,
148 (iv), simulations performed with the commercial code DIANA (2008), where an orthotropic elasto-
149 plastic with softening macroscopic model is adopted for masonry, are also represented to further
150 assess present numerical results. Full details of the latter model may be found in Grande et al.
151 (2008).
152 For the un-strengthened panel (PAN-A), it is interesting to notice that the results obtained using the
153 two-step approach here presented are, near the peak point, almost identical to experimental data,

furnishing also a strength value in very good agreement with DIANA simulations. Also the initial stiffness and the post peak behavior are reproduced very well.

For the strengthened panel PAN-A1, the present model exhibits a force-displacement curve in good agreement with both experimental data and commercial code DIANA simulations, also in the post-peak range. The results obtained for PAN-A2 are again very near to experimental ones, both in terms of peak-strength and post-peak behavior. The acceptable differences between present model and DIANA may be explained remembering that within DIANA the strengthening is modeled by means of truss elements perfectly bonded to the masonry surface, where delamination is accounted for limiting tensile strength to f_{fdd} or $f_{fdd,rid}$ near the anchorage zone, see Part I.

In Figure 2 deformed shapes at peak obtained for PAN-A, PAN-A1 and PAN-A2 series respectively are also represented. As FE simulations show, in PAN-A1 series the horizontal strip acts as a tie. Even though the two-strut model of the un-strengthened case remains essentially unchanged, both the compressed sections increase as well as the intensity. In PAN-A2 deformed shape suggests a change both of the direction of the compressed struts and in the failure mechanism. The deformed shape at collapse shows compression near the supports, shear under the load and delamination of the diagonal strengthening. This is confirmed by the color map of damaged zones in masonry interfaces (normal and shear stresses) reported in Figure 3 and the delamination patch of the reinforcing strip -referred to tangential FRP/masonry interface stresses- registered at peak depicted in Figure 4.

2.2. Diagonally strengthened shear wall

A set of non-strengthened and diagonally strengthened shear walls experimentally tested by Zhao et al. (2004) is analyzed in this section, see Figure 5. The geometry of the shear walls, built with solid clay bricks of dimensions 240 × 115 × 53 mm, is 240 × 1400 × 1000 mm (thickness × length × height), with an aspect ratio (H/L) equal to 0.714. The panels were placed within two precast strengthened concrete beams at the top and the bottom, to preclude rotation of the horizontal edges.

Insufficient information on constituent materials mechanical properties are provided in Zhao et al. (2004). In particular only solid clay brick and mortar compressive strengths are given, which resulted equal to 16.9 MPa and 11.6 MPa, respectively. The remaining material data adopted in this paper to fully characterize the model, see Table I, are chosen in agreement with the experience of the authors and in order to fit as close as possible experimental shear-displacements curves.

Two walls were tested by Zhao et al. (2004) labeled as Wall-1 and Wall-2. Wall-1 is a non-strengthened shear wall, used to check the increase of the load bearing capacity induced by the diagonal strengthening in Wall-2. Wall-2 is a panel strengthened with a so called "Λ" disposition by means of a bi-directional carbon fiber strengthened polymer sheet, cut to four 300 mm wide strips.

During the tests, a constant vertical pre-compression equal to 1.2 MPa was uniformly distributed onto the top of the wall through one distribution beam and 8 solid steel rods. Cyclic lateral loads were applied to the top strengthened concrete beam by a hydraulic jack fixed horizontally on a stiff loading reaction frame. The first loading cycle on both walls was conducted to 30% of the estimated maximum load of the plain wall. The following cycles were used to determine the cracking displacement by adding 20% of the calculated maximum load to Wall-1 and Wall-2, respectively. Then, lateral loading was controlled by multiples of the cracking displacement until the failure of the specimen was reached.

A comparison between numerical response and experimental base shear-top edge horizontal displacement cyclic curves is depicted in Figure 6 for both the non-strengthened and strengthened shear panel. The agreement seems again satisfactory; both the peak and the post peak behavior exhibit basically similar behaviors. As can be noted from Figure 6, the use of composite strips increases considerably the ultimate load carrying capacity. Furthermore, from experimental envelops of the cyclic curves of the load–displacement relations, it can be concluded that the use of FRP can also increase the stiffness, thanks to the fact that fiber sheets delay the propagation of diagonal cracks and restrict the damaged area along diagonal struts.

Deformed shapes at peak of both walls obtained numerically are represented in Figure 7. From experimental crack patterns exhibited by Wall-1 and Wall-2, Zhao et al. (2004) observed that in the strengthened Wall-2 cracks propagated under the strengthening and appeared later with respect to the non-strengthened case. The change of the cracked zone due to the introduction of the diagonal strengthening is particularly clear. This behavior seems well captured by the simple model proposed, also observing the color patches of Figure 7, representing the interfaces inside masonry which undergo damage for tensile and shear stresses. Shear damage concentrates, for the strengthened and non-strengthened case, in the lower part of the panel. However, when FRP strips are added to the structure, a visible concentration may be noted under the right diagonal strip immediately above the base anchorage. Also tensile stress damage increases in the strengthened case, as a consequence of the overall increase of the load bearing capacity, concentrating near the horizontal edges in tensile zone.

Finally, in Figure 7-bottom the delamination patches for tangential interface stresses acting between the strip and masonry are represented. The contribution of the tangential stress perpendicular to FRP direction is separated by that of the stress acting parallel to the strip not only for the sake of clearness but also because in this case the contribution of shear along the horizontal direction is crucial, especially near the top edge. This contribution is observed also in the experimental tests and seems reproduced quite accurately by the model proposed. As a matter of fact, delamination of the strips is observed near the lower anchorage for actions parallel to the strips, together with a diffused detachment of the strengthening near the upper crossing zone.

3. FRP strengthened masonry curved structures

In this Section, two strengthened masonry structures with curved shape are analyzed to assess the capabilities of the numerical approach proposed in presence of combined in- and out-of-plane actions.

229 The first example relies on a circular arch with buttresses and longitudinal strengthening loaded
230 with a horizontal action simulating an earthquake, numerically analyzed by Mahini et al. (2007) in
231 presence and absence of strengthening. The second is a ribbed cross vault –i.e. a double curvature
232 structure- experimentally tested in absence of strengthening by Faccio et al. (1999), and already
233 analyzed in the non-strengthened case by Creazza et al. (2000 & 2002) and by Milani et al. (2009)
234 in the strengthened case within a limit analysis procedure. An experimental campaign was also
235 conducted by Foraboschi (2006) in presence of strengthening in one of the principal arches, but the
236 resultant force-displacement curves are not available.
237 For all the cases discussed, the two-step non-linear approach proposed has been adopted to predict
238 the pushover curve exhibited by the structure, with particular emphasis on the peak load carrying
239 capacity and deformation at failure. Where available, constituent materials -experimentally
240 determined- mechanical properties have been adopted. In absence of specific data available,
241 reasonable literature data have been assumed. Finally, load-displacement curves provided by the
242 model have been compared to results obtained with commercial codes and experimental evidences.

243 ## 3.1. Circular arch with buttresses

244 The vault considered in this Section was numerically analyzed by Mahini et al. (2007) in presence
245 and absence of strengthening. The aim was to have an insight into the behavior of a typical existing
246 roof vault which can be encountered in a heritage complex building in Iran. The system of vaults
247 was built in 1935 by adobe and clay bricks with clay mortar and gypsum-clay mortar, respectively.
248 The vault has a circular shape with radius equal to 3.50 m, see Figure 8, with a span of L equal to
249 6.47 m. Buttresses have an height equal to 3.17 m. Piers and vault thicknesses are equal to 0.9 and
250 0.2 m, respectively. All geometrical dimensions together with the structural components of the arch
251 can be deduced from Figure 8.
252 While the resistance to vertical gravity loads is reasonably good in this type of construction, the
253 lateral resistance is not adequate and, therefore, the performance under seismic loads needs

254 improvements. For this reason, the strengthening intervention shown in Figure 8 is numerically
255 evaluated by Mahini et al. (2007), who modeled the structure with a smeared crack material,
256 available within the commercial code ANSYS (2004).
257 Mechanical properties adopted in the present model for the constituent materials have been already
258 presented in the first part of the paper and are not repeated here for brevity. Here it is worth
259 remembering that they are derived, where possible, from experimental data available. In particular,
260 in Mahini et al. (2007), a wide experimental characterization in compression on brick and gypsum-
261 clay prisms extracted from the original units as a part of the vaults is at disposal.
262 It can be deduced that each prism was made of seven solid clay bricks which had been connected by
263 1:1 gypsum-clay mortar. From in-situ observations, it can be deduced that the relatively low tensile
264 bond strength between the bed joint and the unit caused tensile failure of the composite masonry.
265 Therefore, the masonry tensile strength can be assumed to be equal to the tensile bond strength
266 between the joint and the unit. In this paper, the tensile strength of mortar reduced to interfaces is
267 assumed equal to mortar/brick strength and is deduced from four points bending test conducted by
268 Mahini et al. (2007) on small masonry pillars. Piers are constituted by a different material, being
269 built with adobe and clay mortar. In the model, homogenization is obviously by-passed for the piers
270 and an isotropic elasto-plastic material is utilized. Again some experimental data (full stress-strain
271 diagrams) in compression on new adobe piers -each prism consisted of four adobe units connected
272 by clay mortars- may be collected from Mahini et al. (2007). Tensile strength of adobe piers was
273 also measured using a similar testing set-up for brick prisms.
274 Numerical simulations are performed applying self-weight and an increasing lateral load, constantly
275 distributed along the height of piers, simulating roughly a seismic load proportional to the mass, as
276 shown in Figure 8 and in agreement with Mahini et al. (2007). In order to investigate the seismic
277 upgrading of the circular arch obtained through a FRP strengthening, the structure is supposed
278 retrofitted with one strip of composite material placed at the extrados of the arch and two short
279 strips on the surfaces of the piers subjected to tension, as in Figure 8. The width of strip is equal to

20 cm. Uni-directional CFRP strips are used, possessing a tensile strength of about 3900 MPa, an elastic modulus equal to 240 GPa and an ultimate tensile elongation of 1.55%. The thickness of fiber laminate is 0.165 mm. When the saturant is cured, the thickness of CFRP laminate becomes 1mm.

The lateral behavior of the vault in terms of base shear-maximum horizontal displacement is illustrated -in presence and absence of strengthening- in Figure 9. Only a comparison with numerical results obtained by Mahini et al. (2007) using the commercial code ANSYS and limit analysis collapse loads provided by an upper bound FE approach proposed by the first author (see e.g. Milani et al. 2009) is possible here. In any case, again the global behavior seems in satisfactory agreement with alternative numerical procedures. Here it is worth noting that the total lateral load carrying capacity of the non-strengthened vault is around 31.2 kN, whereas for the strengthened case passes 40 kN. The retrofitting scheme proposed provides therefore a 30% increase in the load carrying capacity, whereas the maximum horizontal displacement decreases (percentage difference around 20%). This is completely in agreement with the FRP architecture, which aims for an increase in strength rather than ductility capacity.

In Figure 10 deformed shape at peak obtained with the numerical approach proposed are represented for both the strengthened and the non-strengthened case. Without FRP, the arch fails for the formation of relatively well defined cylindrical hinges (H1, H2, H3 and H4), three located along the arch (H2, H3 and H4) and the latter (H1) at the base of the right pier. Hinge H3 is located near the center of the arch. This is not surprising because the vertical load is relatively small, the structure with horizontal load only is anti-symmetric and the central section therefore exhibits a null pre-compression. The small axial force is due only to gravity loads and the section fails for very little bending (again due to vertical loads). The remaining two hinges on the arch are again, as expected, in anti-symmetric disposition. No prediction may be attempted for the piers because their pre-compression is sensibly higher. The position and diffusion of the hinges is well represented by the damage map on masonry interfaces depicted in Figure 11.

306 The strengthening is obviously placed in tensile region on piers and at the extrados on the arch, in
307 such a way to preclude the hinges opening. H3 remains near the middle span at the intrados. As a
308 matter of fact here the strengthening has little influence, being disposed in the compression fiber of
309 the section. The opening of such hinge seems more defined if compared to the non-strengthened
310 case. Again H2 forms at the top edge on the right of the arch, but the damaged region diffuses
311 considerably, as a consequence of the action of the strip which tend to preclude the extrados
312 opening (see damage map in Figure 11). On the contrary, H4 does not for on the arch, since its
313 opening is precluded by the FRP and moves from the arch to the base of the left pier. This is a clear
314 consequence of the strengthening, which tends also to diffuse the damage near the base of both
315 piers in correspondence of hinges H1 and H4, accompanied by a considerable delamination of the
316 strips.
317 FRP delamination map is represented in again Figure 11 for the sake of completeness. As can be
318 noted also analyzing the deformed shape at peak (Figure 10), FRP delaminates near the supports
319 and in correspondence of H2 hinge on the arch, in tensile zone. This behavior is again in agreement
320 with experimental evidences and code of practice recommendations (CNR DT-200 2004 and
321 Focacci 2008).

322 ## 3.2. Cross Vault

323 A ribbed cross vault, experimentally tested in the non-strengthened case by Faccio et al. (1999) and
324 with FRPs by Foraboschi (2006), formed by the intersection of two barrel vaults with external
325 radius of 2.3 m, is consider as fourth example. The geometry of the vault is depicted in Figure 12,
326 along with its FE discretization. Strengthening strips disposed at the intrados and extrados of the
327 boundary arch near the point of application of the load are also visible.
328 Common Italian bricks of dimensions $120 \times 250 \times 55$ mm^3 were used to build the vault, with joints
329 thickness equal to 10 mm. Mechanical properties adopted for the constituent materials are

summarized in Table II and, where possible are taken in agreement with literature data, see for instance Milani et al. (2009).

The vault is loaded vertically with a concentrated force increased up to collapse and placed eccentrically. When dealing with the non-strengthened case, the experimental crack pattern exhibited by the structure includes three well defined cylindrical hinges on the ribbed arch near the point of application of the wall and a limited punching under the loaded area. Numerical results obtained with a macroscopic continuum non-linear model (similar to that implemented in DIANA 2008) are also available from Creazza et al. (2000 and 2002) in the non-strengthened case.

To partially preclude the formation of the failure mechanism, a double intrados-extrados FRP strengthening is disposed by Foraboschi (2006) in correspondence of the boundary ribbed arch near the point of application of the load, as in Figure 12.

A synopsis of the numerical results obtained with the present model in presence and absence of strengthening is reported from Figure 13 to Figure 16.

In particular, in Figure 13, a comparison among load-maximum displacement curves provided by a number of different non-linear models (present approach, Creazza et al. 2002, DIANA 2008) is presented, along with experimental data (force-displacement curve) and upper bound collapse load provided by the present model when rigid plastic materials are assumed, see also Milani et al. (2009). The increase in the load bearing capacity of the structure after the introduction of the strips is rather clear. Unfortunately, no information on collapse load reached experimentally is available in the FRP strengthened case. For this reason, in the strengthened case, the performance of the present model may be compared only with commercial code predictions and limit analysis results.

In Figure 14, deformed shapes at peak provided by the approach proposed are represented in presence and absence of strengthening. In absence of strengthening the failure mechanism –in good agreement with experimental evidences- shows a mixed shear flexural failure of the nail and the arch near the load. This is confirmed by the masonry damage patch for normal stress and shear, reported respectively in Figure 15 and Figure 16. The three plastic hinges (one placed in

correspondence of the symmetry axis and the others at approximately 1/3 of the arch span) developing in the ribbed arch are rather clear in the non-strengthened case. A well defined curved sliding surface may be also noted from Figure 16. Obviously, the introduction of the FRP strengthening precludes the easy formation of the flexural hinges on the ribbed arch and diffuses damage inside the nail, facilitating out-of-plane sliding. Indeed, a marked punching of the area under the external load is visible. This is confirmed both by the deformed shape (see the detail in Figure 14) and the damage map, Figure 15 and Figure 16. In the strengthened structure, as expected, normal stress damage diffuses on contiguous ribbed arches.

In Figure 16 FRP-masonry interfaces delamination patch is also represented for the sake of completeness. As expected, damage concentrates near the anchorage zones and in correspondence of the hinges in tensile zones in correspondence of the ribbed arch near the load.

4. Conclusions

A simple two-step 3D model for the evaluation of the non-linear behavior of FRP strengthened masonry structures has been presented. In Part I, a homogenization approach was utilized in the non-strengthened case, step one, to obtain non-linear stress-strain relationships to use at a structural level, step two.

Here, four structural examples have been extensively analyzed, supposing to apply FRP strips on an already homogeneous masonry material, exhibiting orthotropic behavior with softening, known from the first step.

At a structural level, masonry has been modeled by means of rigid infinitely resistant wedge elements interconnected by non-linear orthotropic interfaces. FRP strips have been modeled by means of triangular rigid elements. To properly take into account the brittle delamination of the strips from the support, it has been supposed that masonry and FRP layers interact by means of interfacial tangential actions between triangles (FRP) and wedges (masonry), following an elastic behavior with a degradation of the strength until zero in correspondence of a pre-defined slip, in

agreement with available codes of practice formulas. Linear piecewise constant approximations of all the stress-strain relationships have been assumed to solve the incremental elasto-plastic problem within non-linear programming approaches. In this way, the delamination phenomenon at the FRP/masonry interface and masonry failure may be taken into account suitably.

To assess the numerical model proposed, several numerical examples have been analyzed, namely two different typologies of masonry in-plane loaded (a set of deep beams variously strengthened and a shear wall), a circular arch and a ribbed cross vault.

From simulations results it appears that sufficiently reliable predictions of both peak loads and deformation history have been obtained with both approaches, at a fraction of the time needed by standard FEM.

5. References

[1] ANSYS. User's Manual, 9th ed., SAS IP, Inc. 2004.

[2] CNR-DT 200 (2004). Guide for the design and construction of externally bonded FRP systems for strengthening existing structures. C.N.R. National Research Council, Italy.

[3] Creazza G, Saetta A, Matteazzi R, Vitaliani R (2000). Analyses of masonry vaulted structures by using a 3-D damage model. European Congress on Computational Methods in Applied Sciences and Engineering, ECCOMAS 2000, Barcelona, SP.

[4] Creazza G, Saetta A, Matteazzi R, Vitaliani R (2002). Analyses of masonry vaults: a macro approach based on three-dimensional damage model. Journal of Structural Engineering 128(5): 646-654.

[5] D.M. (1987) Norme tecniche per la progettazione, esecuzione e collaudo degli edifici in muratura e per il loro consolidamento. Italy. 1987.

[6] DIANA 9.3 version User's Manual (2008). TNO Building and Construction Research, Department of Computational Mechanics, Delft, The Netherlands.

405 [7] Faccio P, Foraboschi P, Siviero E (1999). Masonry vaults reinforced with FPR strips [In
406 Italian: Volte in muratura con rinforzi in FRP]. L'Edilizia 7/8: 44-50.

407 [8] Fedele, R., Milani, G. (2011). "Three-dimensional effects induced by FRP-from-masonry
408 delamination." Composite Structures 93(7): 1819-31.

409 [9] Focacci, F. Rinforzo delle murature con materiali compositi [Masonry strenghtening with
410 composite materials]. Flaccovio; 2008.

411 [10] Foraboschi P (2004). Strengthening of masonry arches with fiber-reinforced polymer strips.
412 Journal of Composites for Construction 8: 191-202.

413 [11] Foraboschi P (2006). Masonry structures externally reinforced with FRP strips: tests at the
414 collapse [in Italian]. In: Proc. I Convegno Nazionale "Sperimentazioni su Materiali e
415 Strutture", Venice, 2006.

416 [12] Grande, E., Milani, G., Sacco, E. (2008). Modelling and analysis of FRP-strengthened
417 masonry panels. Engineering Structures, 30 (7), 1842-1860.

418 [13] Korany, Y., Drysdale, R. (2007). Load-Displacement of Masonry Panels with Unbonded and
419 Intermittently Bonded FRP. I: Analytical Model. J. Compos. for Constr. 11(1): 15-23.

420 [14] Lourenço, P. B. (2000). "Anisotropic softening model for masonry plates and shells." J.
421 Struct. Eng., 126(9), 1008–1016.

422 [15] Luciano, R., Sacco, E. (1998). Damage of masonry panels reinforced by FRP sheets. Int J
423 Solids Struct 35(15):1723–41.

424 [16] Mahini, S.S., Ronagh, H.R. and Eslami, A. (2007). Seismic rehabilitation of historical
425 masonry vaults using FRPs: A case study. In *Proc.* 1st Asia-Pacific Conference on FRP in
426 Structures (APFIS 2007), S.T. Smith (Ed), University of Hong Kong and International
427 Institute for FRP in Construction (IIFC), Hong Kong, China, 12-14 December 2007, 1: 565-
428 570.

[17] Marfia, S., Sacco, E. (2001). Modelling of reinforced masonry elements. Int J Solids Struct 38:4177–98.

[18] Massart T, Peerlings RHJ, Geers MGD (2004). Mesoscopic modeling of failure and damage-induced anisotropy in brick masonry. Eur J Mech A/Solids 23: 719–35.

[19] Mercatoris BCN, Massart TJ, Bouillard P (2009). Multi-scale detection of failure in planar masonry thin shells using computational homogenisation. Eng Fract Mech 76(4): 479-499.

[20] Milani G, Lourenço PB (2010). Monte Carlo homogenized limit analysis model for randomly assembled blocks in-plane loaded. Computational Mechanics 46(6): 827-849.

[21] Milani G, Milani E, Tralli A (2009). Upper Bound limit analysis model for FRP-reinforced masonry curved structures. Part II: structural analyses. Computers & Structures 87 (23-24): 1534–1558.

[22] Moon, F.L., Yi, T., Leon, R.T., Khan, L.F. (2007). Testing of a full scale unreinforced masonry building following seismic strengthening. ASCE J Struct Eng 133(9): 1215–26.

[23] Mosallam, A.S. (2007). Out-of-plane flexural behavior of unreinforced red brick walls strengthened with FRP composites. Composites Part B: Engineering 38 (5-6): 559-574.

[24] Ramos, L.F., Lourenço, P.B. (2004). Advanced numerical analysis of historical centers: A case study in Lisbon, Engineering Structures 26(9): 1295-1310

[25] Triantafillou, T.C. (1998). Composites: a new possibility for the shear strengthening of concrete, masonry and wood. Compos Sci Technol 58:1285–95.

[26] van der Pluijm, R. (1992). Material properties of masonry and its components under tension and shear. In: Proc. 6th Canadian masonry symposium.

[27] Yi, T., Moon, F.L., Leon, R.T., Khan, L.F. (2006). Lateral load tests on a two story unreinforced masonry building. ASCE J Struct Eng 132(5): 643–52.

452 [28] Zhao, T., Zhang, C., Xie, J. (2004). Shear behavior of UCMW using CFRP sheet: a case
453 study. TMS Journal September 2004, 90-96.

Figures

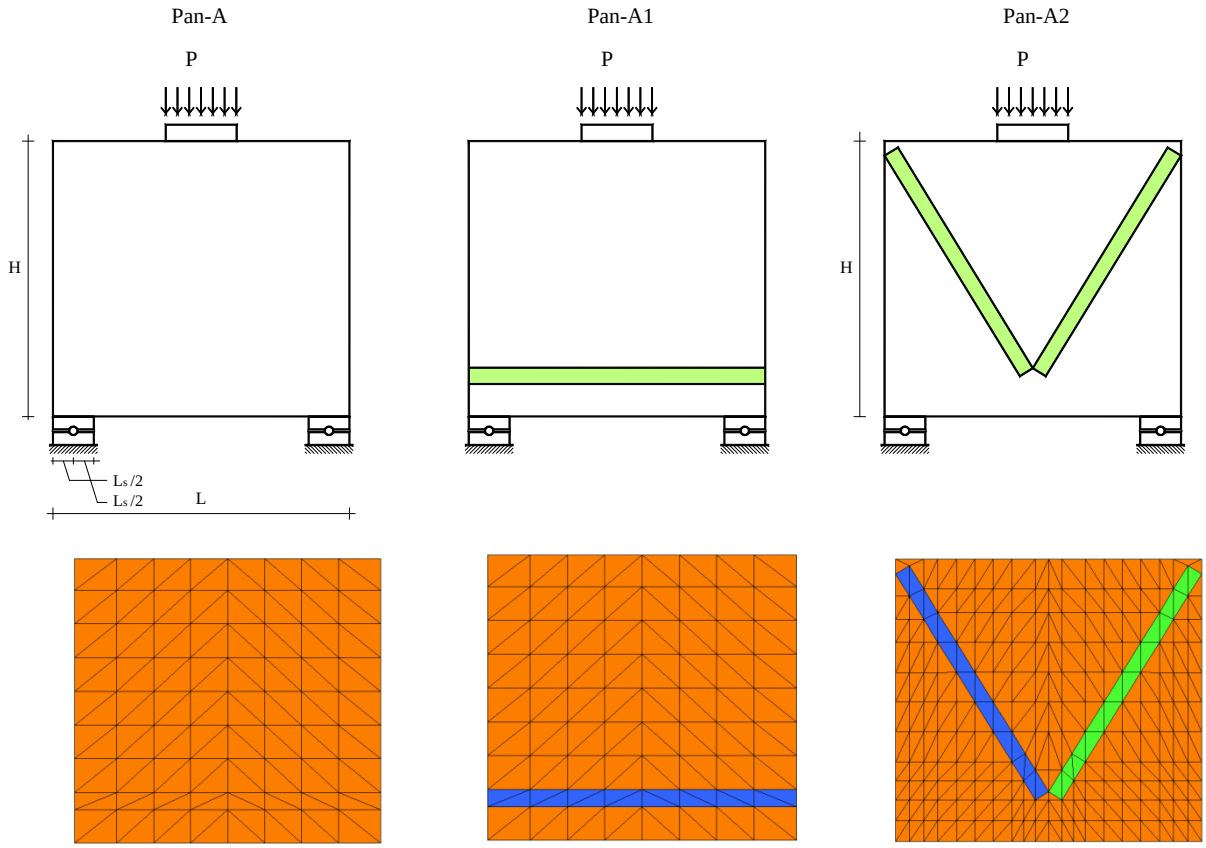

Figure 1: Masonry deep beam. Geometry, loading condition and FE discretization adopted for the numerical analyses.

Pan-A

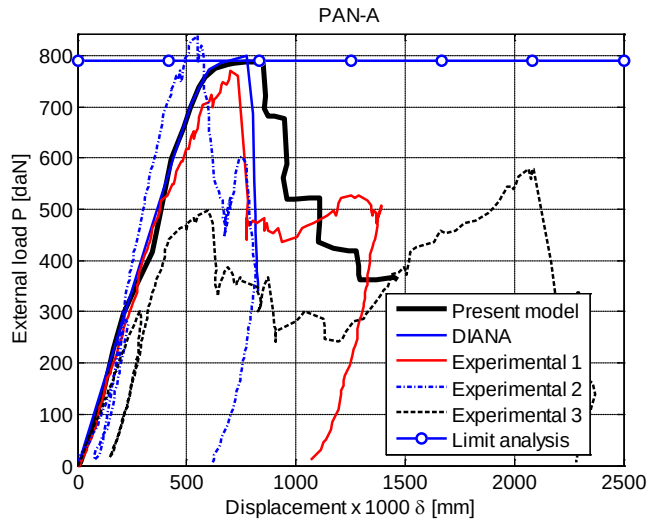

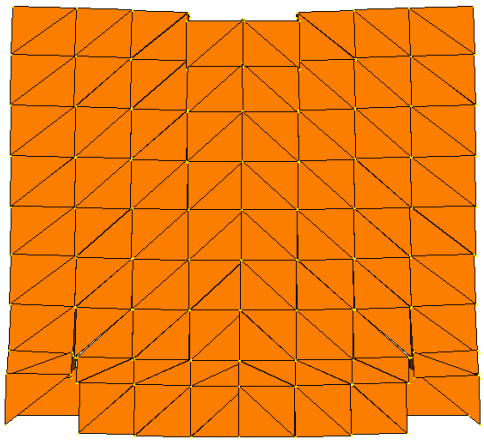

Pan-A1

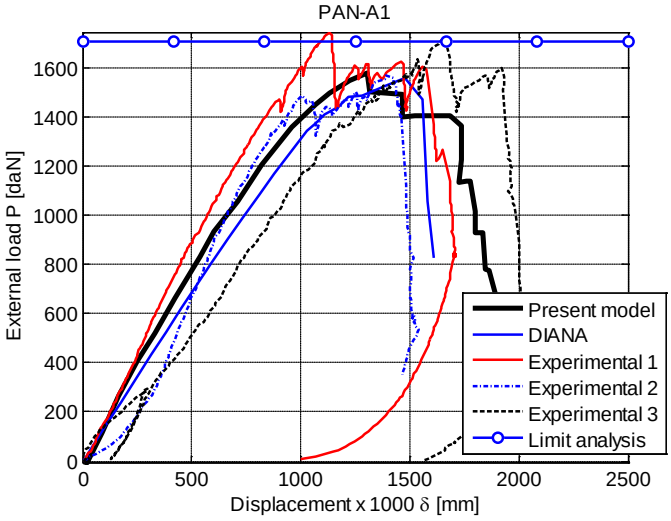

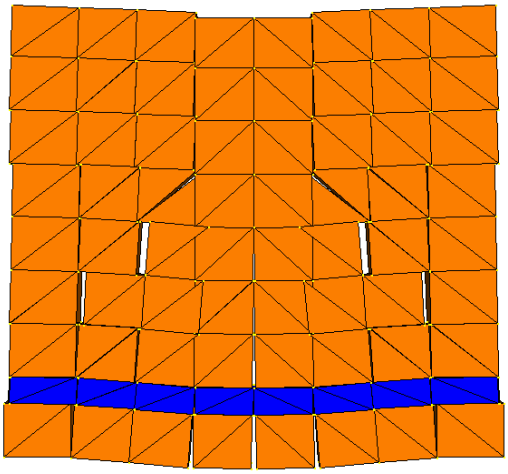

Pan-A2

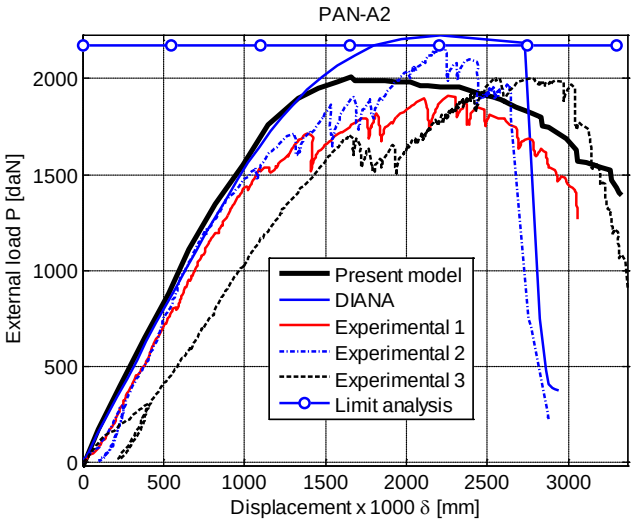

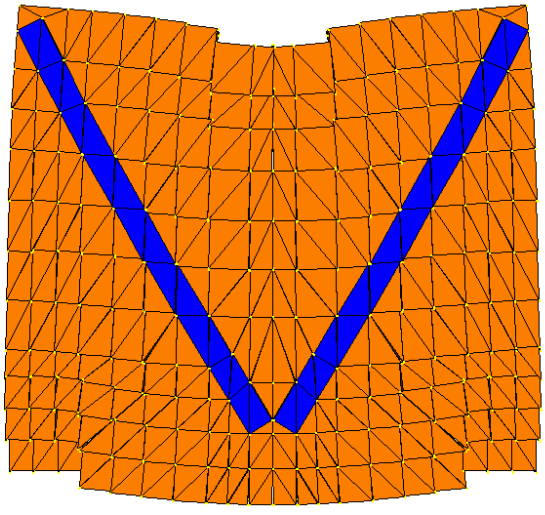

Figure 2: Masonry deep beam. Left: Comparison among load-displacement curves or collapse loads provided by experimentation, limit analysis and non-linear FE codes (commercial and present software). Right: Deformed shapes at peak

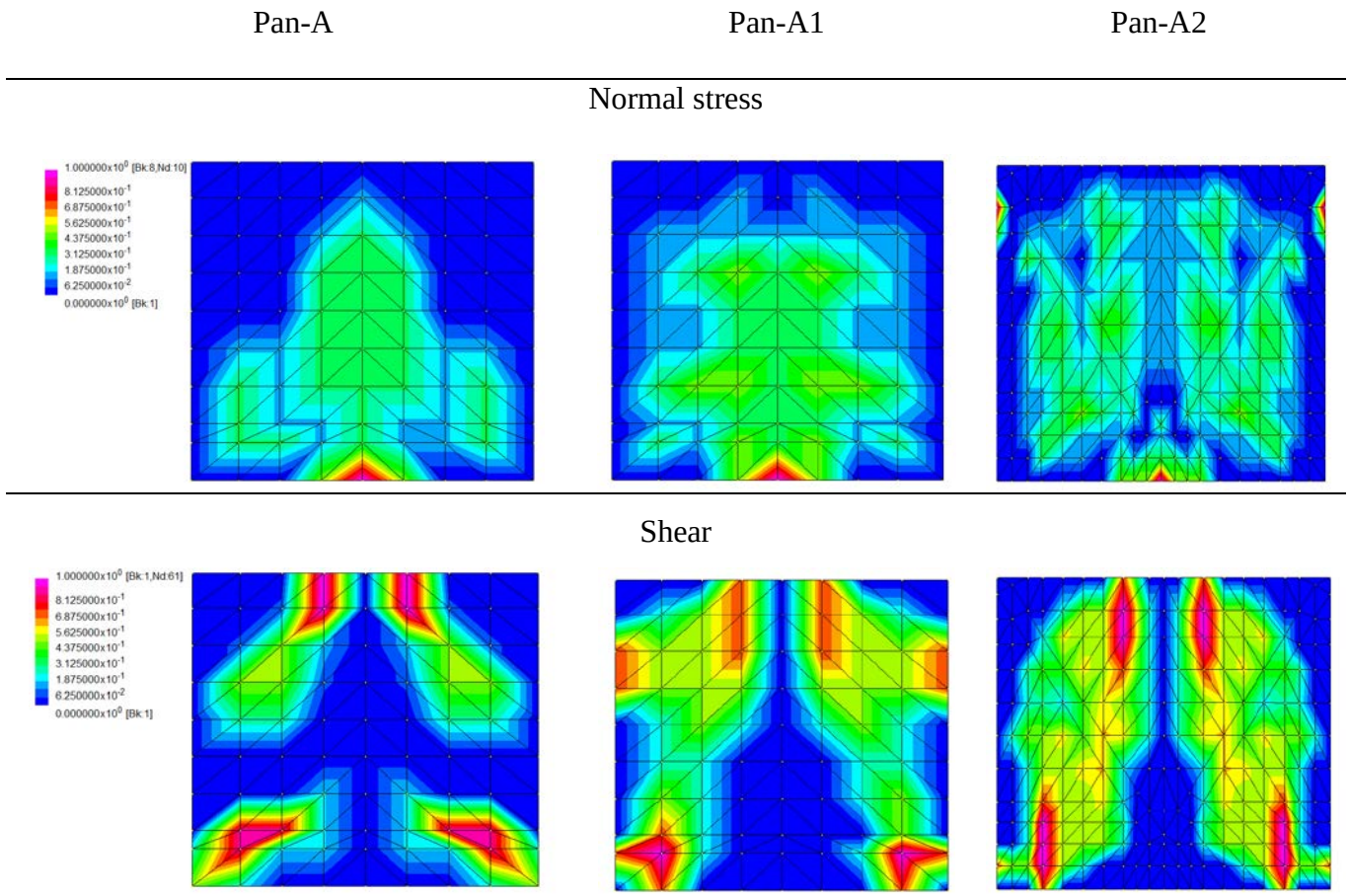

Figure 3: Masonry deep beam. Degraded interfaces patch for normal and shear stress (from 0 -no degradation- to 1 –full degradation) obtained through the non-linear homogenized FE code proposed.

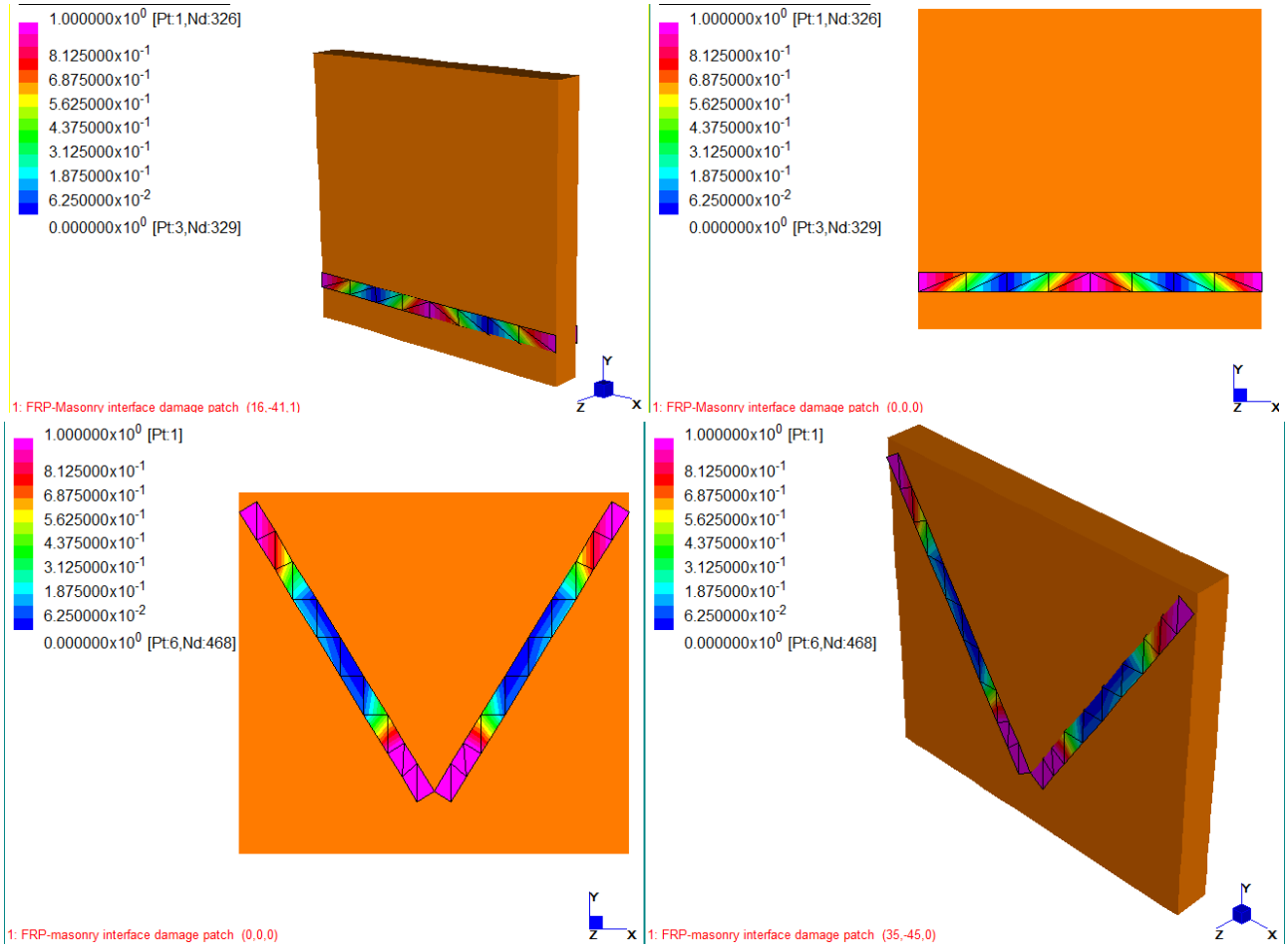

Figure 4: Masonry deep beam. Degraded FRP-masonry interfaces patch for shear action (from 0 -no degradation- to 1 –full degradation) obtained through the non-linear homogenized FE code proposed (top: Pan-A1. Bottom: Pan-A2).

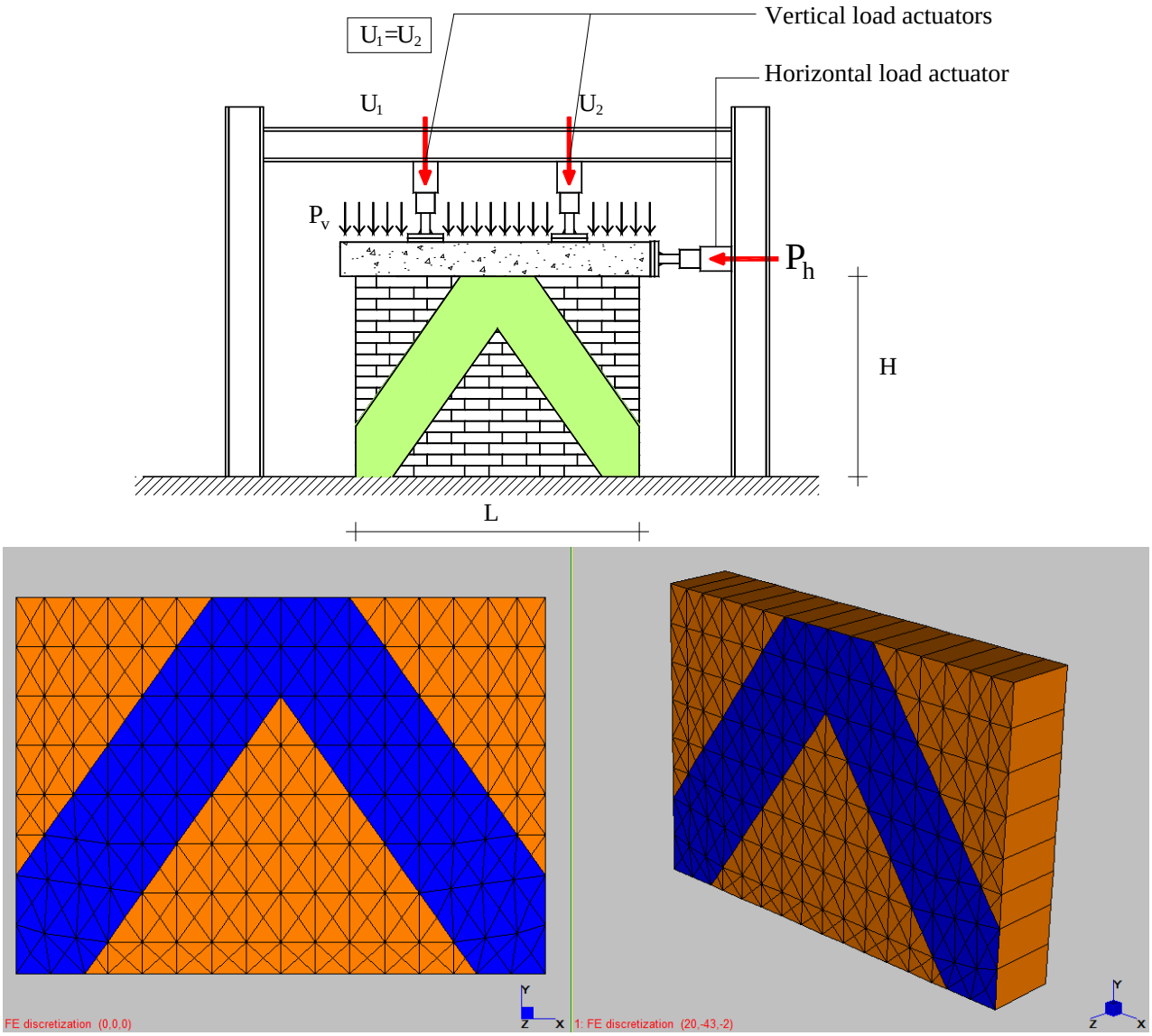

Figure 5: Strengthened shear wall. Geometry, loading condition and FE discretization adopted for the numerical analyses.

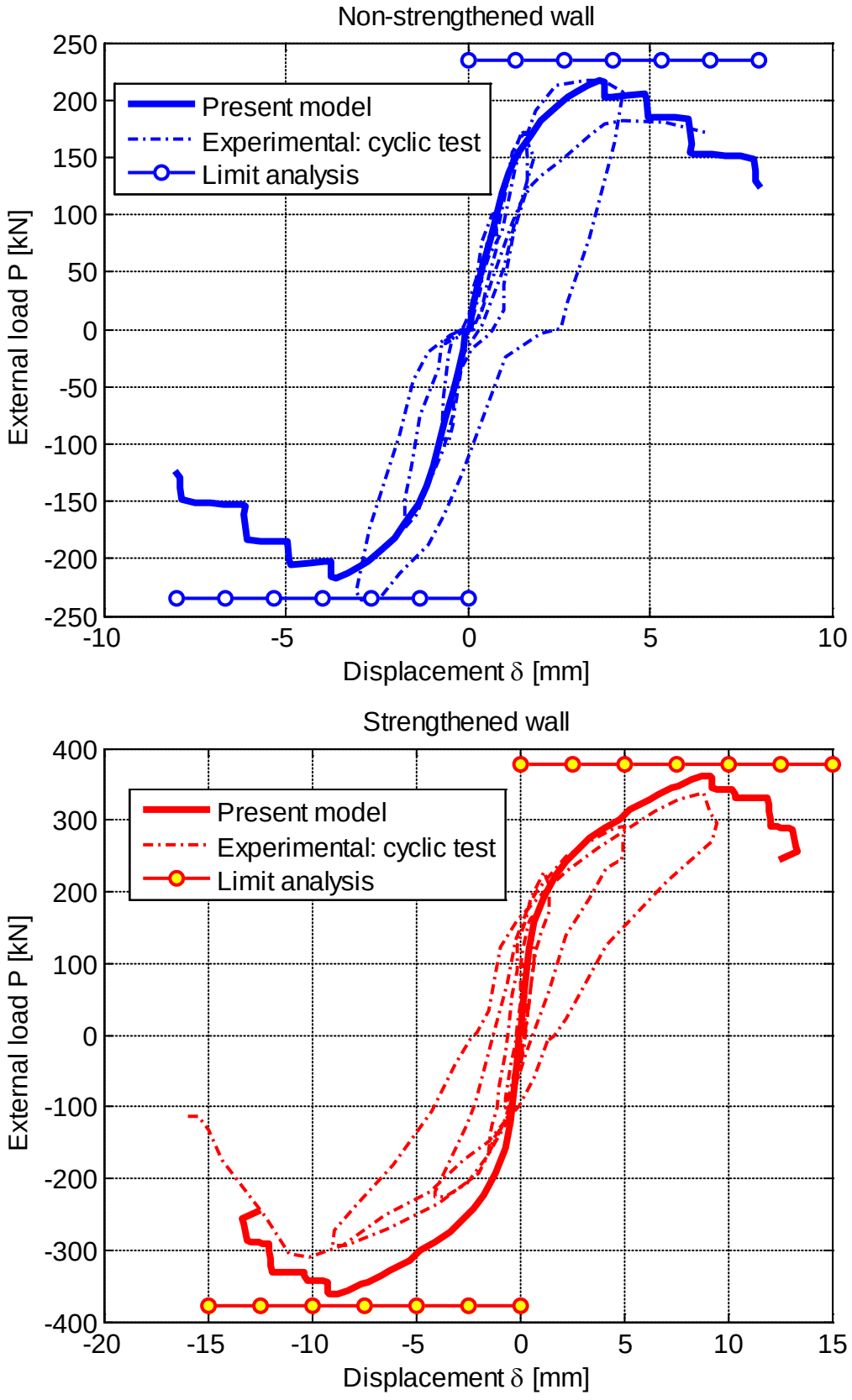

Figure 6: Strengthened shear wall. Comparison between cyclic load-displacement curves provided by experimentation and non-linear FE code.

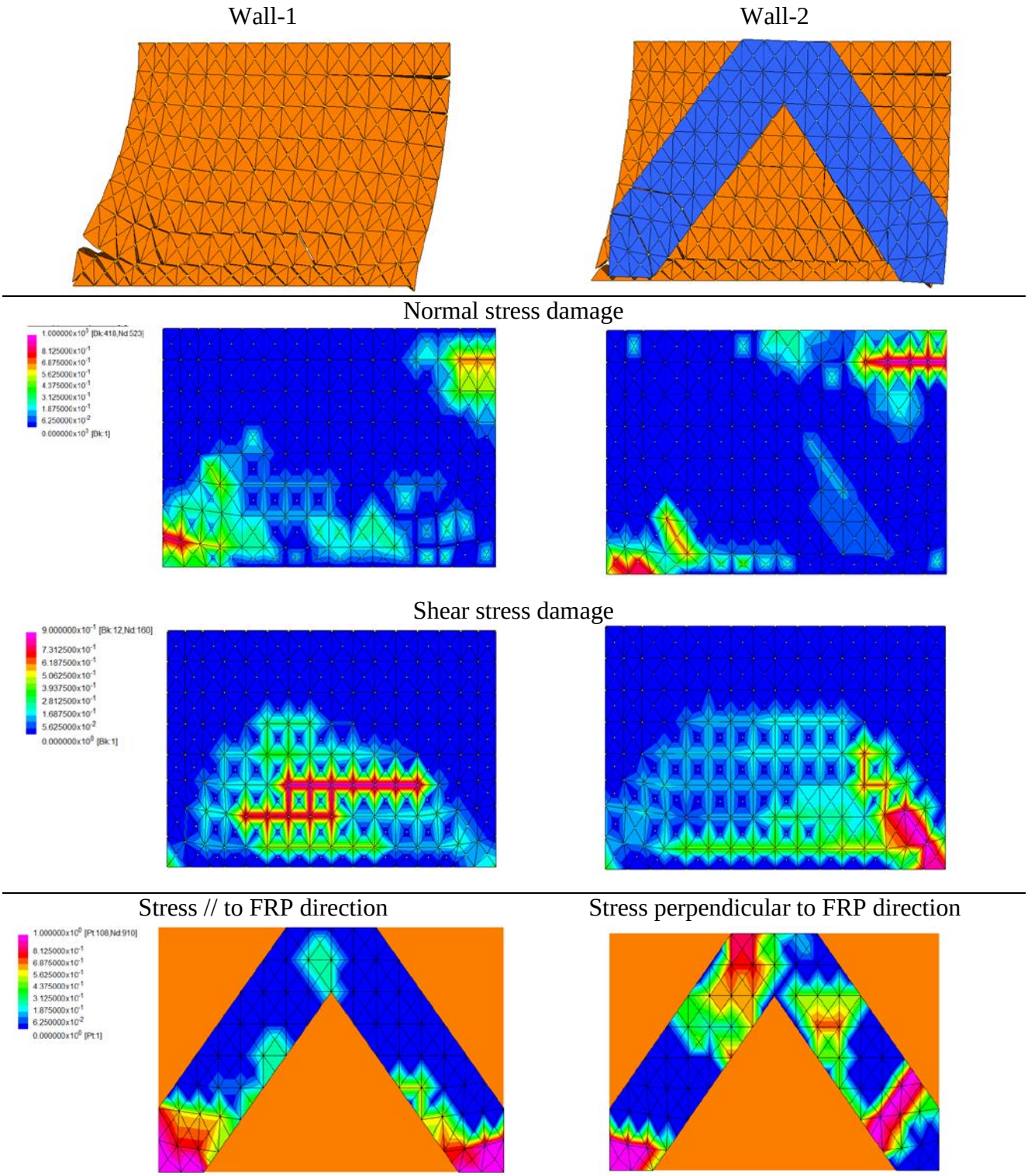

Figure 7: Strengthened shear wall. Top: Deformed shapes at peak provided by the proposed non-linear code. Center: normal and shear stress damage map. Bottom: FRP masonry delamination map.

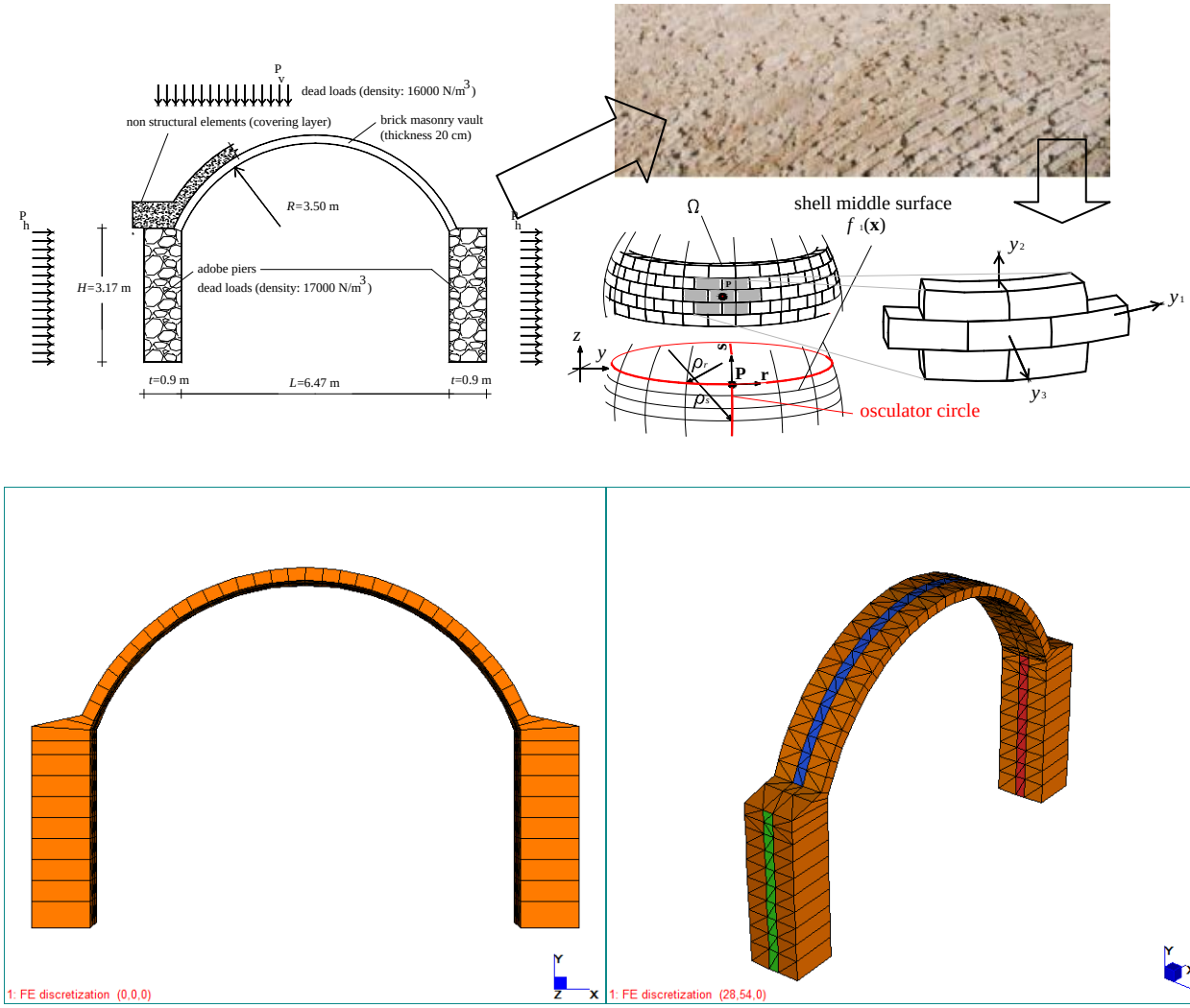

Figure 8: Circular arch with buttresses. Geometry, loading condition and FE discretization adopted for the numerical analyses.

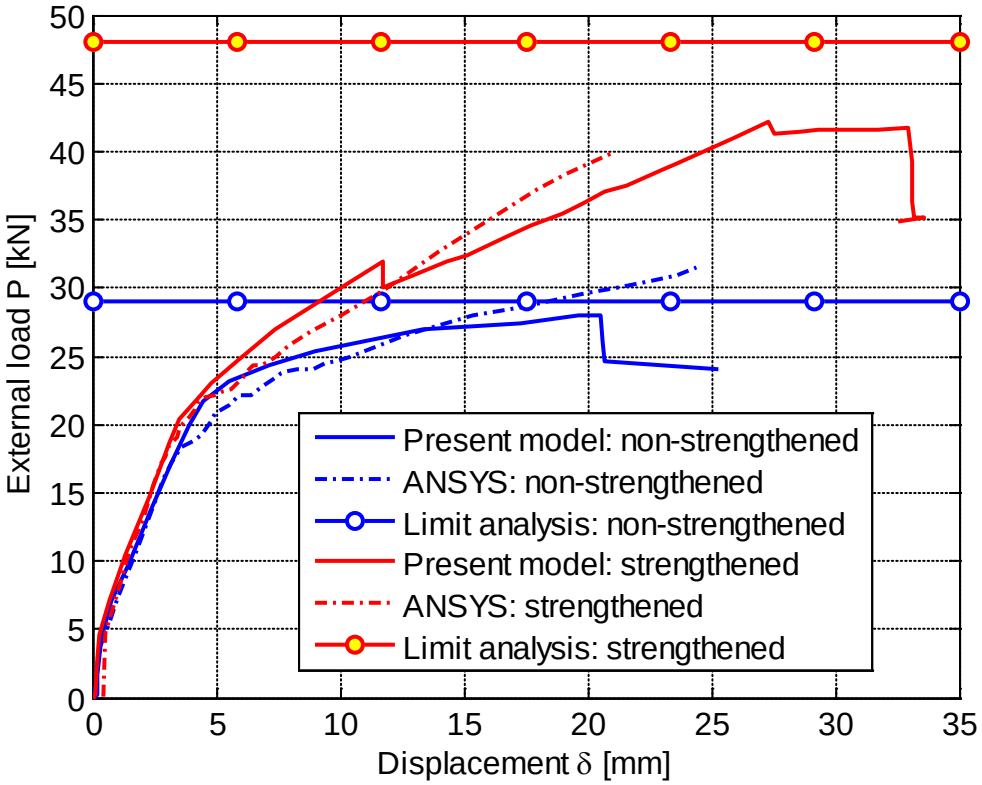

Figure 9: Circular arch with buttresses. Comparison among load-displacement curves provided by commercial code, ultimate loads provided by limit analysis and present non-linear FE code.

Non-strengthened arch

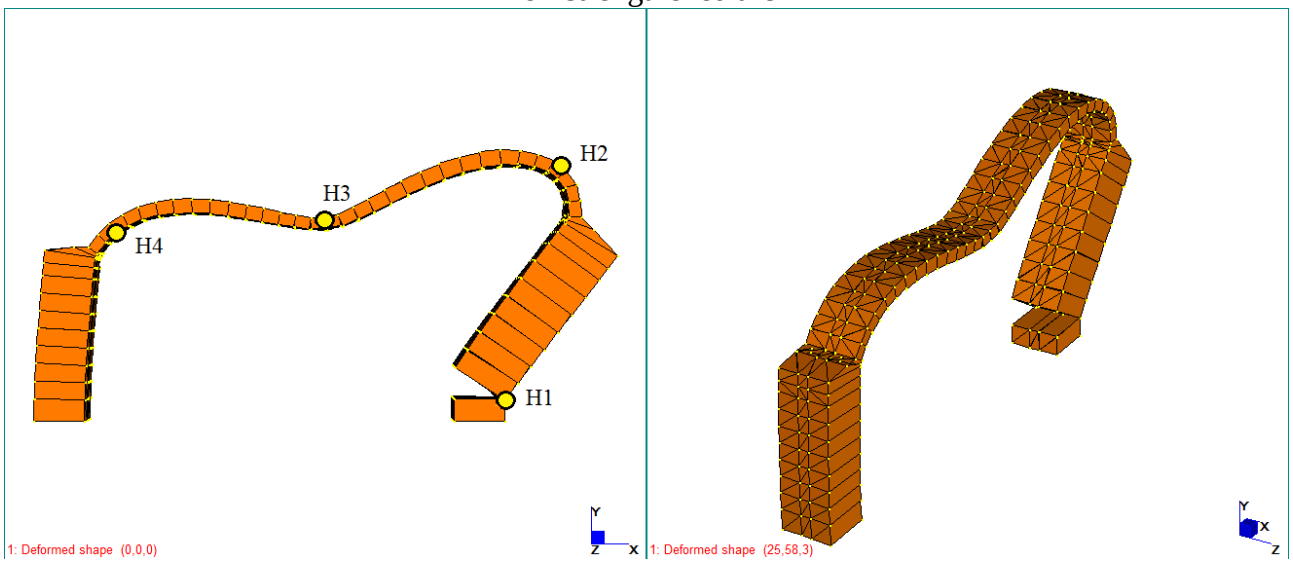

Strengthened arch

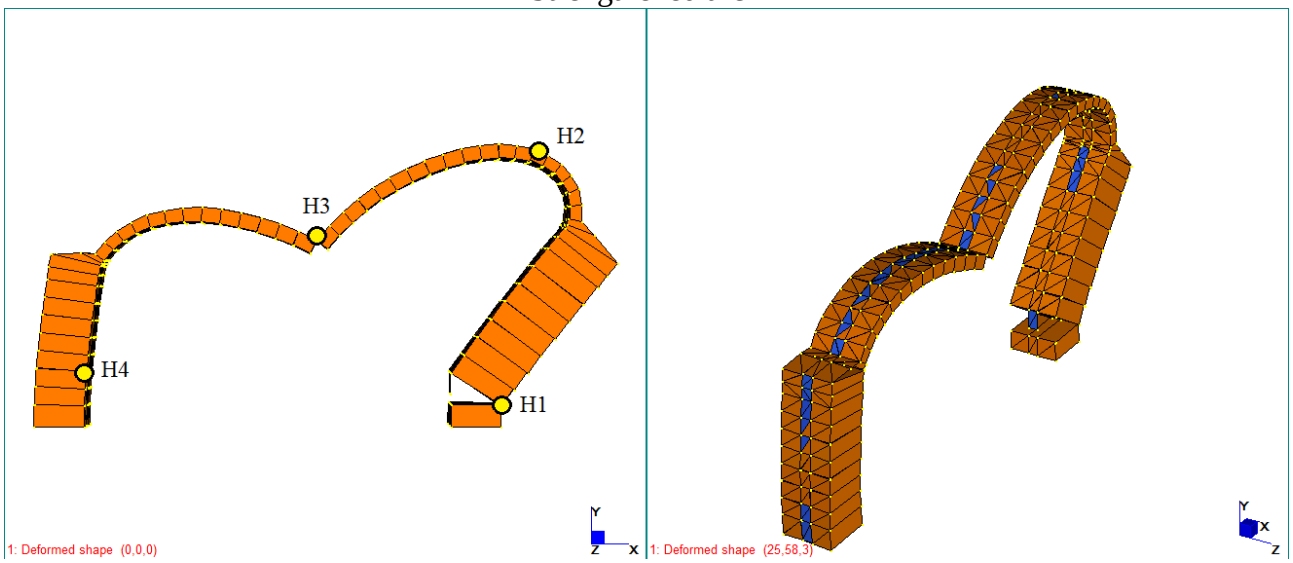

Figure 10: Circular arch with buttresses. Deformed shapes at peak provided by the proposed non-linear code.

Non-strengthened arch

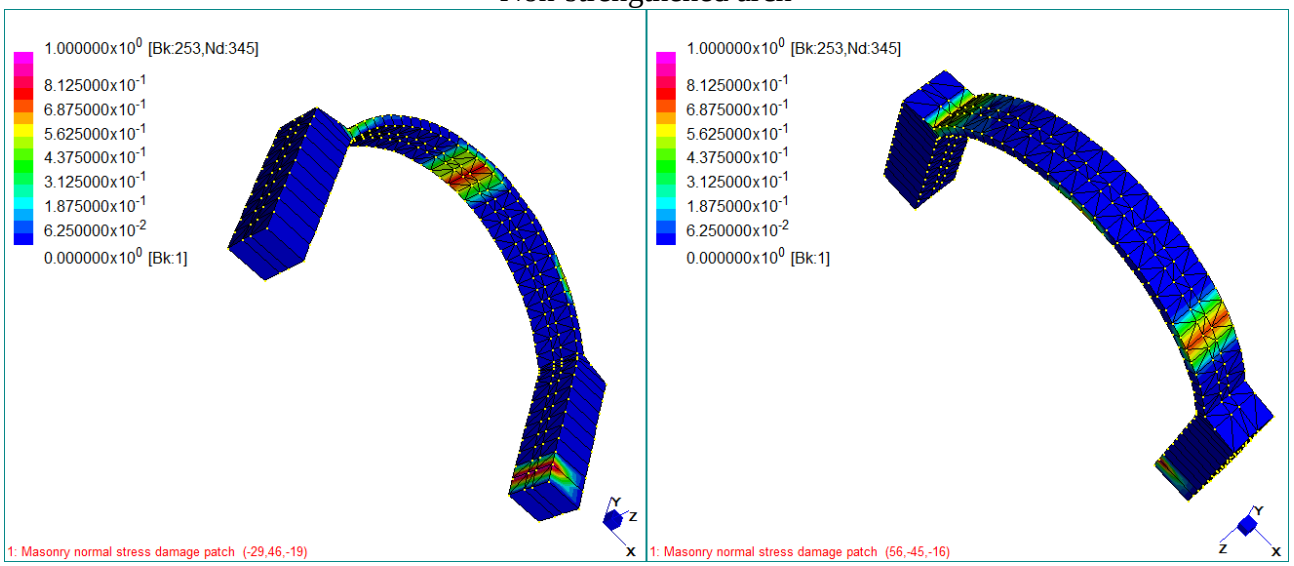

Strengthened arch

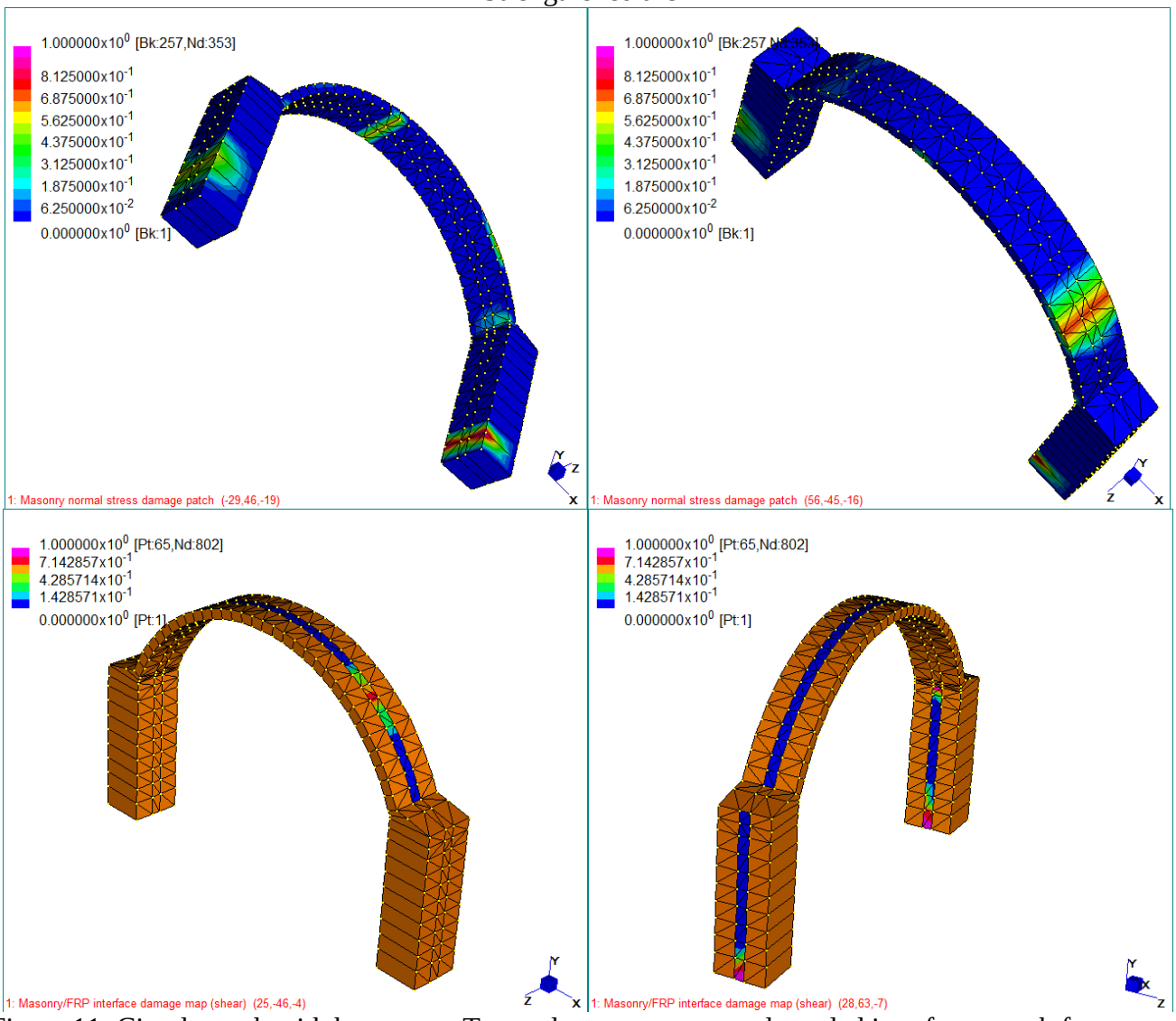

Figure 11: Circular arch with buttresses. Top and center: masonry degraded interfaces patch for normal stress action (from 0 -no degradation- to 1 –full degradation). Bottom: FRP delamination patch for shear stress.

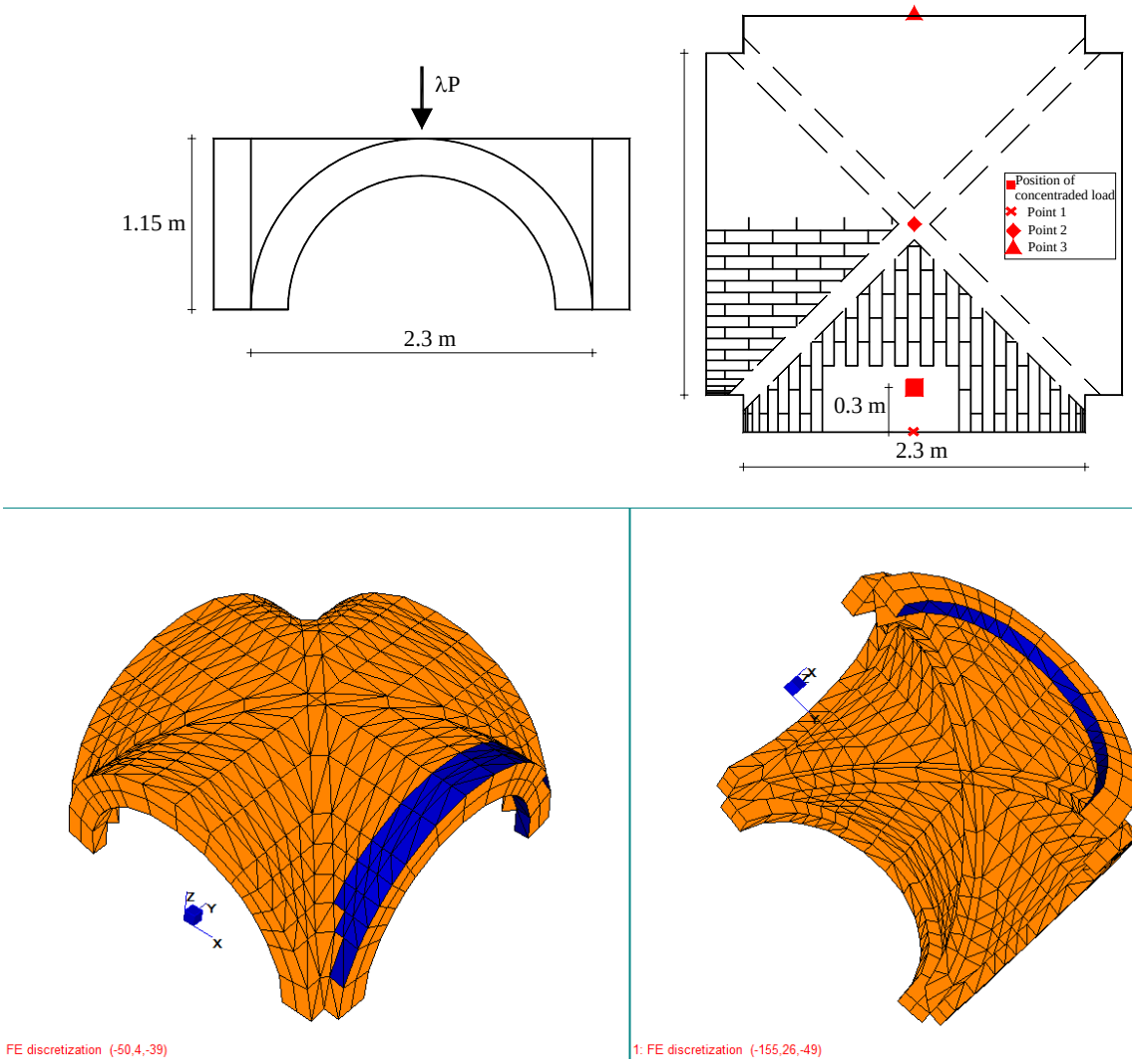

Figure 12: Ribbed cross vault. Geometry, loading condition and FE discretization adopted for the numerical analyses.

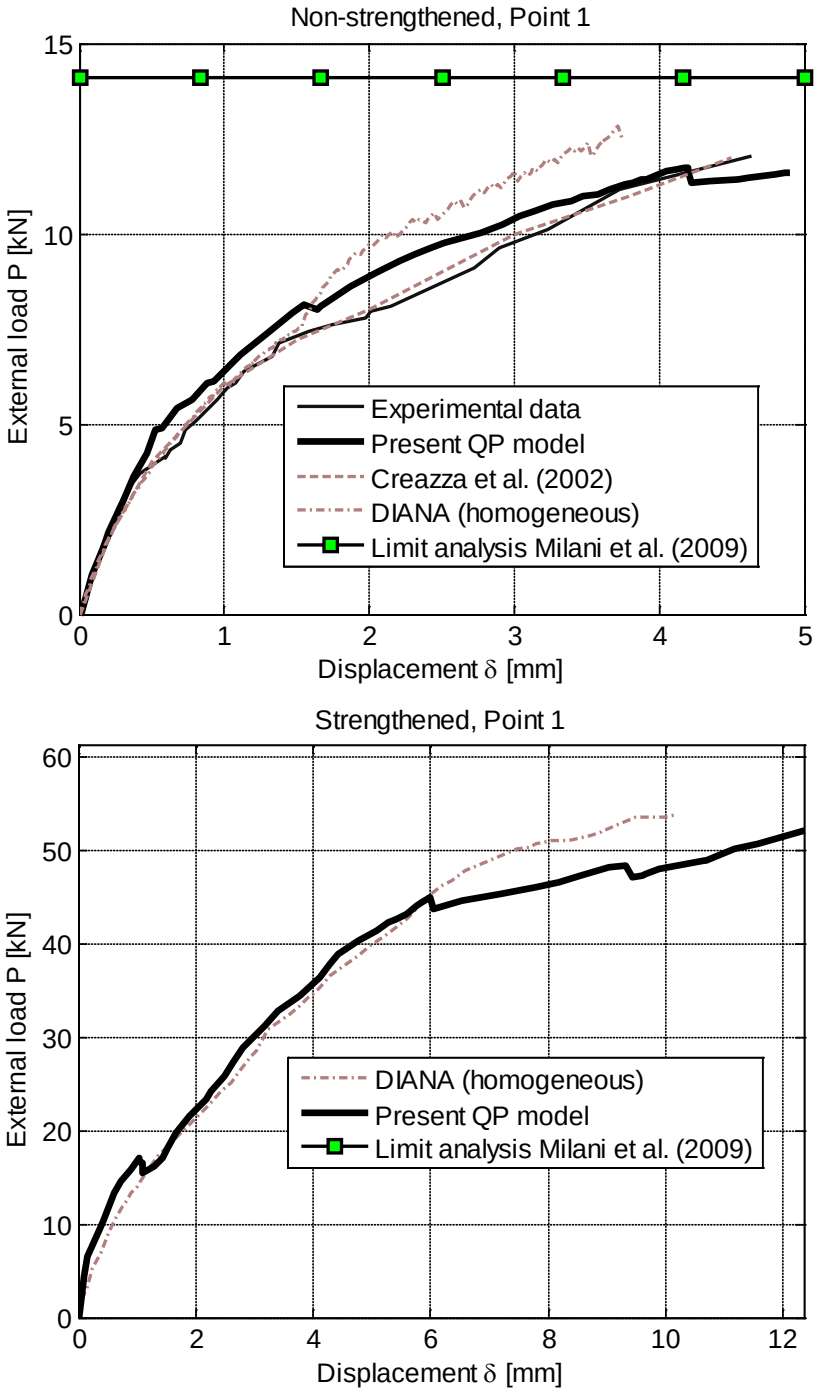

Figure 13: Ribbed cross vault. Comparison among load-displacement curves or collapse loads provided by experimentation, limit analysis and non-linear FE codes (commercial codes and present results).

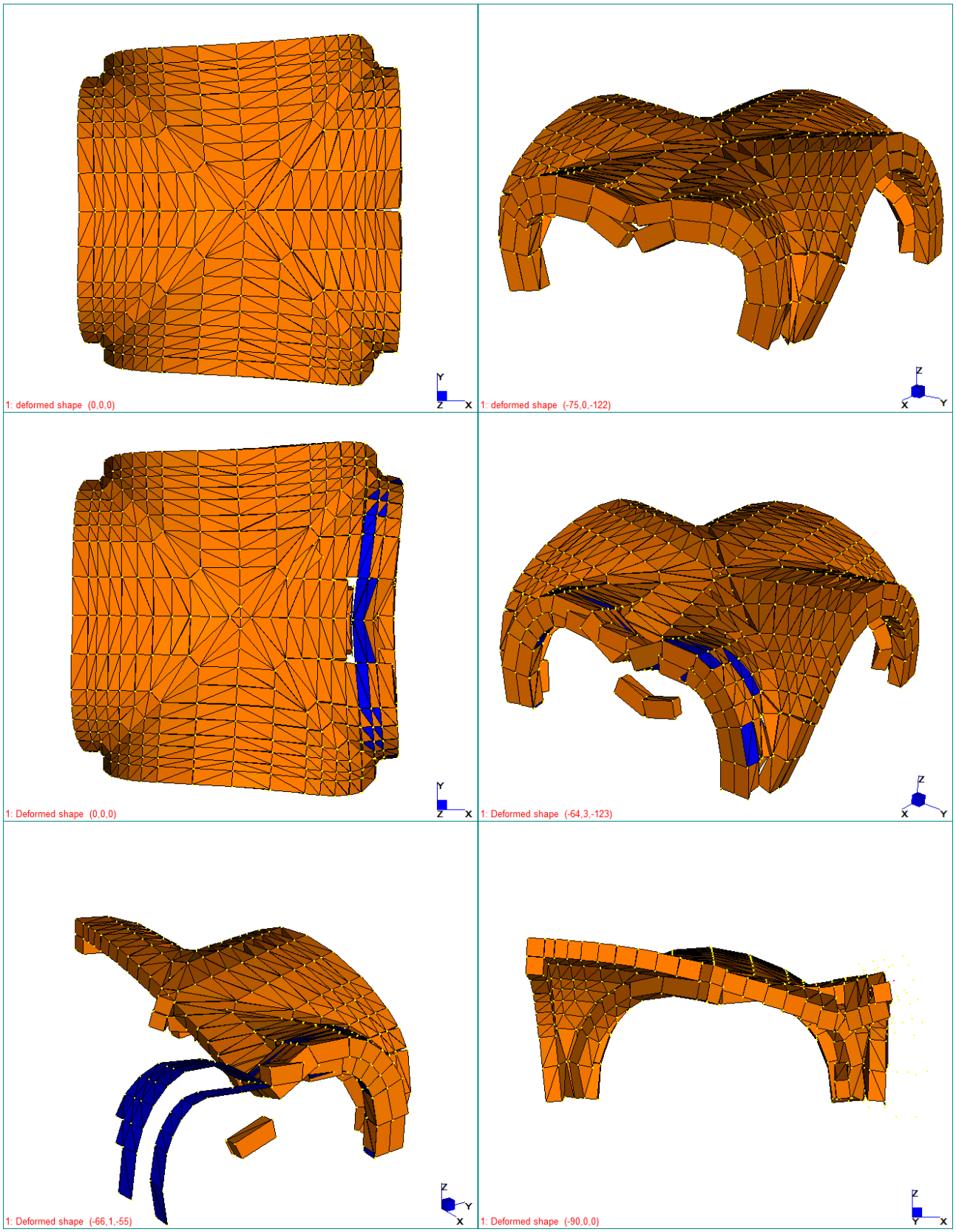

Figure 14: Ribbed cross vault. Deformed shapes at peak provided by the proposed non-linear code and detail of the out-of-plane sliding in the strengthened case (bottom).

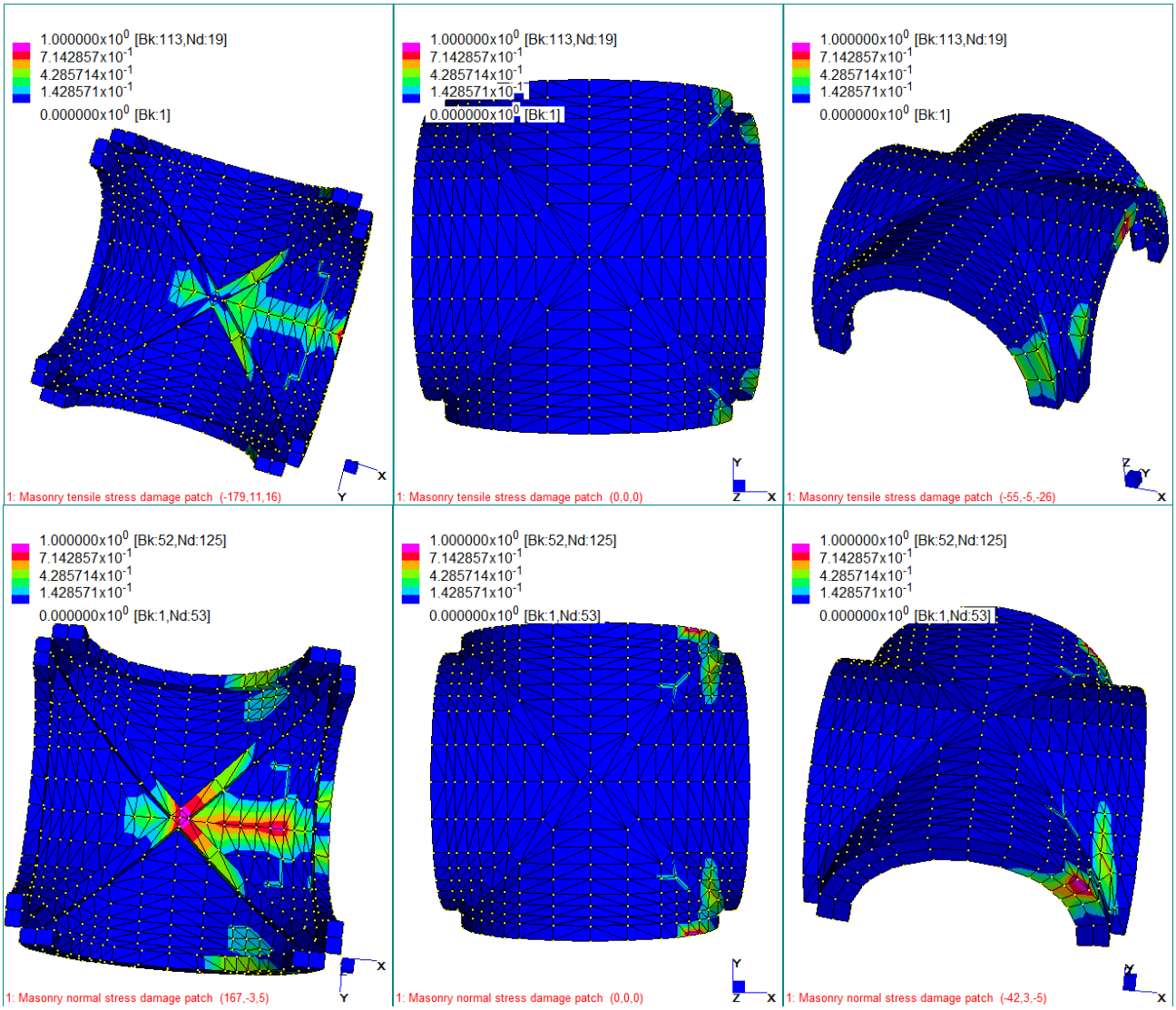

Figure 15: Ribbed cross vault. Positive normal stress degraded interfaces patch (from 0 -no degradation- to 1 –full degradation) obtained through the non-linear homogenized FE code proposed. Top: non-strengthened. Bottom: strengthened.

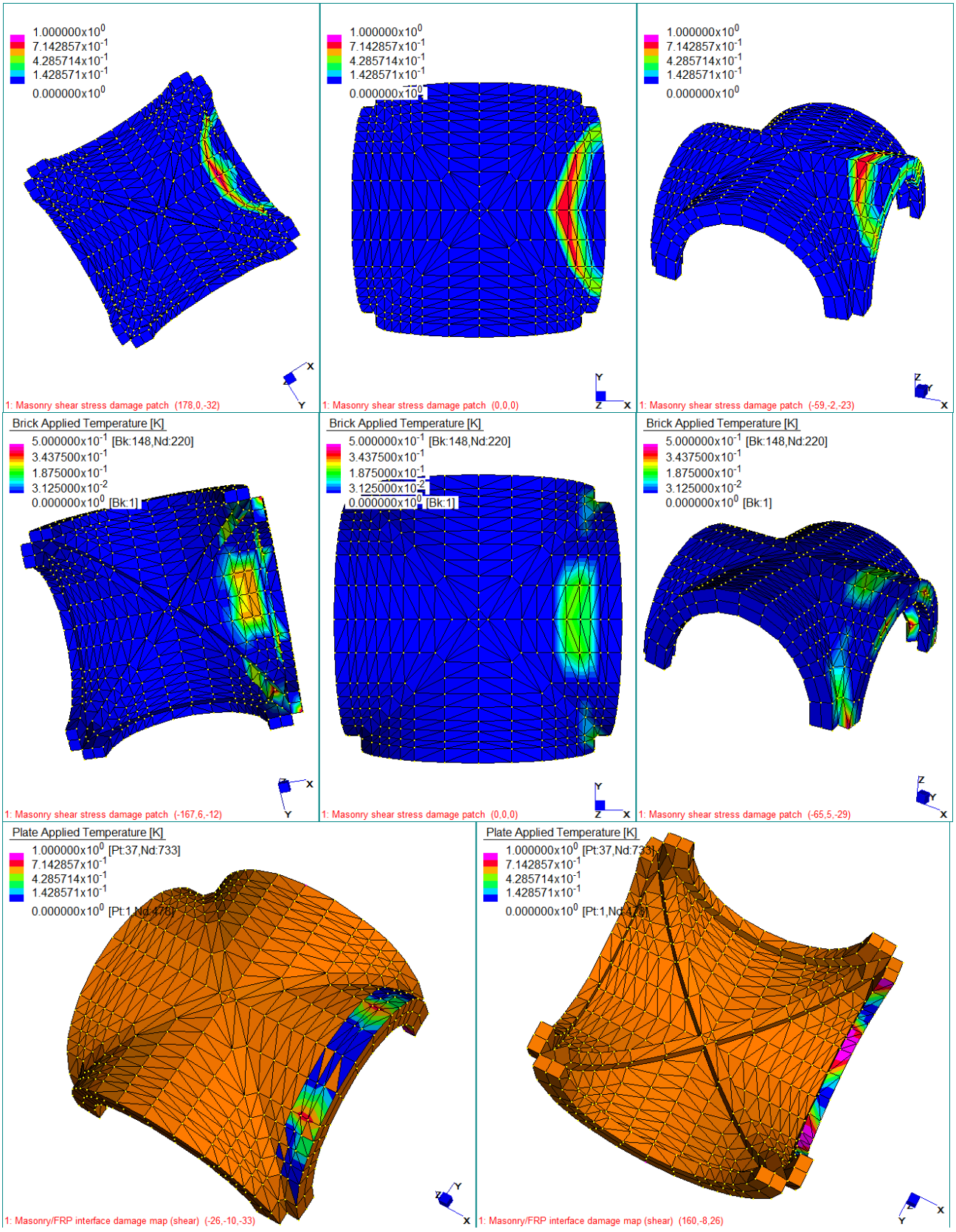

Figure 16: Ribbed cross vault. Shear stress degraded interfaces patch (from 0 -no degradation- to 1 – full degradation) obtained through the non-linear homogenized FE code proposed. Top: non-strengthened. Center: strengthened. Bottom: FRP-masonry interfaces delamination patch.

Tables

Table I: Strengthened shear wall. Mechanical properties adopted for constituent materials.				
	joint	brick-brick interface		
E	1200(*)		[MPa]	Young Modulus
G	810(*)		[MPa]	Shear Modulus
c	1.0 f_t	2	[MPa]	Cohesion
f_t	0.30	-	[MPa]	Tensile strength
f_{ce}	$1/3 f_{cp}$	-	[MPa]	Compressive hardening/softening behavior
f_{cp}	11.6	-	[MPa]	
f_{cm}	$0.75 f_{cp}$	-	[MPa]	
f_{cr}	$1/2 f_{cp}$	-	[MPa]	
κ_p / e_h	0.009	-	[-]	
κ_m / e_h	0.049	-	[-]	
Φ	30	45	[°]	Friction angle
Ψ	60	-	[°]	Angle of the linearized compressive cap
G_f^I	0.0065	10	[N/mm]	Mode I fracture energy
G_f^{II}	0.0050	10	[N/mm]	Mode II fracture energy
FRP masonry interfaces				
Kn	20		[N/mm^3]	Young Modulus
Kt	8		[N/mm^3]	Shear Modulus
c	0.4		[MPa]	Cohesion
f_t	1		[MPa]	Tensile strength
du	0.03		[mm]	Ultimate slip
(*) Values referred to masonry				

Table II: Ribbed cross vault. Mechanical properties adopted for constituent materials.				
	joint	brick-brick interface		
E	1600(*)		[MPa]	Young Modulus
G	900(*)		[MPa]	Shear Modulus
c	1.0 f_t	2	[MPa]	Cohesion
f_t	0.04	-	[MPa]	Tensile strength
f_{ce}	1/3f_{cp}	-	[MPa]	Compressive hardening/softening behavior
f_{cp}	2.6	-	[MPa]	
f_{cm}	1/2f_{cp}	-	[MPa]	
f_{cr}	1/7f_{cp}	-	[MPa]	
κ_p / e_h	0.01	-	[-]	
κ_m / e_h	0.05	-	[-]	
Φ	35	45	[°]	Friction angle
Ψ	90	-	[°]	Angle of the linearized compressive cap
G_f^I	0.0050	10	[N/mm]	Mode I fracture energy
G_f^{II}	0.0010	10	[N/mm]	Mode II fracture energy
FRP masonry interfaces				
Kn	20		[N/mm^3]	Young Modulus
Kt	8		[N/mm^3]	Shear Modulus
c	0.3		[MPa]	Cohesion
f_t	f_t		f_t	f_t
du	0.03		[mm]	Ultimate slip
(*) Values referred to masonry				